Advancing CAD-Based Wing Geometry Optimization Using High-Accuracy Sensitivity Analysis

L. Tönjes, S. Dähne, Prof. Dr. C. Hühne
(German Aerospace Center, Germany)

Abstract

A key enabler in designing highly efficient aircraft is multi-disciplinary optimization (MDO), which considers multiple disciplines simultaneously. The disciplines share information through interdisciplinary gradients.

In aircraft wing design, structure and aerodynamics are the most tightly coupled disciplines. These two disciplines share information through the wing geometry. This makes the parameters related to geometry interdisciplinary.

A well-established method of deforming wing geometries is the free-form-deformation. However, accurately translating changes of design variables to the control points can be challenging. This can create inconsistencies across multiple disciplines, resulting in poorly conditioned optimizations.

In contrast, this work employs a CAD-based approach to alter geometries. Parameters of the CAD model can be directly used as design variables for the MDO, mitigating the need to translate design variables onto control points. Additionally, by using a centralized CAD model, it ensures that multiple disciplines share and utilize the same information effectively.

Previous studies that utilized the CAD-based method typically relied on finite differences to compute sensitivities. While this technique offers simplicity and ease of implementation, it has been observed to negatively impact the convergence rate of the optimization process. This circumstance is addressed using a specialized CAD kernel providing high precision algorithmic differentiation techniques and a process to propagate the surface gradients through the structural optimization.

The benefit of numerical exact geometrical gradients is demonstrated on a wing box use case, where a combined structural and geometrical optimization reduces the mass by 1.1% and converges within roughly half of the iterations needed compared to finite difference gradients.

1. Introduction

Multidisciplinary optimization (MDO) has emerged as a critical approach in the design of aircraft wings, enabling the simultaneous consideration of aerodynamic performance and structural integrity. This integrative method is essential in addressing the complex interactions between disciplines, optimizing the overall wing performance rather than focusing on isolated aspects. It was previously shown that through the use of an MDO early in the design process, better and more cost efficient results can be achieved [1, 2]. Due to the complexity of MDOs, gradient-based optimization algorithms are particularly well-suited, as they locate optimal solutions efficiently. Accurate determination of interdisciplinary gradients, particularly between the structural and aerodynamic domains, is important to this process due to their strong interdependence. These gradients, which represent sensitivities to changes in the wing geometry, are crucial for guiding gradient based optimization algorithms toward optimal solutions.

Many shape parametrization techniques exist that are suitable for MDO applications [3]. Among these, the free form deformation (FFD) approach stands out as one of the most prominent method in recent research [4–7]. This technique originates from computer graphics and is used for morphing images and models by manipulating control points.

The FFD approach is well-suited for MDO because it allows gradients to be calculated using analytical methods. A set of design variables can be employed to deform the geometry, thereby reducing the number of required variables. However, a downside of this method is that the FFD parameters might lack significant meaning to designers and may need to be translated into concrete aerodynamic shape parameters [3]. This translation could lead to inconsistencies across different disciplines if not using the same algorithm for conversion.

Moreover, after deformation with FFD, the resulting geometry exists only as a deformed mesh and must be translated back into CAD data to continue further design processes [8, 9]. In contrast, a CAD-based approach eliminates this additional step by directly using its parameters as design variables, with the CAD data itself driving the geometry changes, resulting in an optimized CAD model at the end of the process. Furthermore, the design variables have a physical significance if the model is constructed correctly. Using a centralized CAD model across multiple disciplines ensures consistency among them.

Most CAD kernels are often not free to use and operate behind a black box, making it difficult to extract sensitivities for gradient-based optimization. Therefore, finite differences (FD) are frequently employed, due to their external perturbation capability. However, FD methods exhibit errors that negatively affect optimization convergence due to noise [8]. To address this

issue, this work utilizes a differentiated CAD kernel, based on *OpenCASCADE Technology* [10], developed by the *German Aerospace Center* (DLR), which is capable of providing numerically exact gradients using algorithmic differentiation (AD) [9, 11].

For structural optimizations, the *lightworks* optimization framework [12] from the DLR provides a framework specialized in the structural optimization of composite wing structures. It offers flexibility through the integration of multiple optimization algorithms, constraints, and design variables.

To facilitate CAD-based geometry optimization, *lightworks* requires the ability to process CAD models and integrate the geometric gradients in the structural optimization.

The methodology section describes the *lightworks* optimization framework and explains how a model for the optimization process is derived from a CAD input and how the geometric gradients are obtained through a node mapping approach. The implementation is verified through its application to a well-known, rectangular box use case from the literature, while analytical gradients serve as a reference.

This work demonstrates the application of AD CAD-based geometric gradients in structural optimization and show a decrease in structural mass, when considering geometrical changes. The efficiency of the algorithmic differentiation is demonstrated by comparing it to the finite difference method, showing a better convergence rate in terms of the number of iterations required.

2. Methodology

To employ a CAD-based approach for structural optimization, it is essential to generate a structural model from CAD data. This automated process ensures that the generated model accurately reflects the CAD design and can be effectively optimized within the *lightworks* framework.

Furthermore, since *lightworks* has previously focused on optimizing structures based solely on structural parameters without considering geometry parameters, an extension to its gradient calculation capabilities is necessary. This enhancement allows for the integration of geometry changes directly into the optimization process. Consequently, any modifications in geometry are now properly accounted for in both the structural constraints and the objective function.

Structural model generation

The structural model is based on parametric CAD data. From this data, the structural model is generated, with each surface in the CAD data representing an optimization region within the structural model. For the structural analysis, a finite element mesh is automatically generated using the open-source tool *Gmsh* [13] based on the provided CAD data.

During the gradient calculation step, nodes are utilized to determine how geometric changes affect the structural constraints and objective function. Structured meshes are used for computational efficiency in this context. The connectivity between optimization regions is ensured through the sharing of common nodes. For a fully functional FE model, additional data such as model constraints, loads, and material properties are appended to the generated mesh.

Figure 1 illustrates this step, showing the generated FE model on the right, which was created from the CAD model on the left side. This generated model is subsequently used by *lightworks* to perform finite element analyses and derive element stresses for criteria analysis during the optimization process.

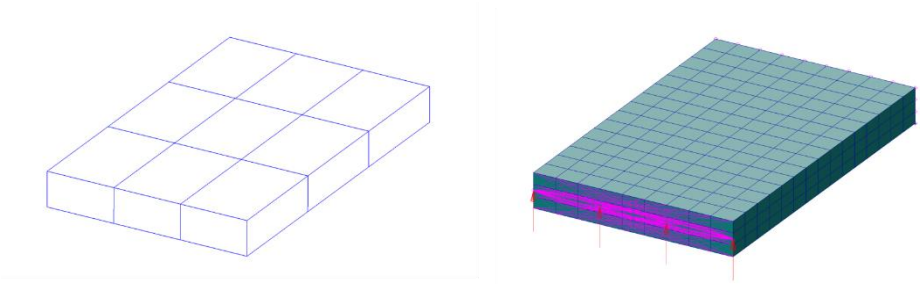

Figure 1: Generation of FE model (right) from CAD model (left)

Node mapping

Each node is capable of being assigned to one or more surfaces. An optimization region within *lightworks* is represented as a surface in the CAD model. Each node in the model is assigned parametric (u, v)-coordinates based on the respective panel. These coordinates are stored during the initial setup or after every geometry change performed by the optimization algorithm (Figure 2, step 1). These two-dimensional coordinates are utilized to map the nodes onto the corresponding three-dimensional surface, where each position on the surface can be assigned a parametric coordinate.

Following any changes to the overall geometry, the underlying panels remain intact but are repositioned (Figure 2, step 2). Consequently, when the geometry undergoes modifications, these nodes can still be accurately mapped back onto

the new geometric configuration using their pre-stored parametric coordinates (Figure 2, step 3).

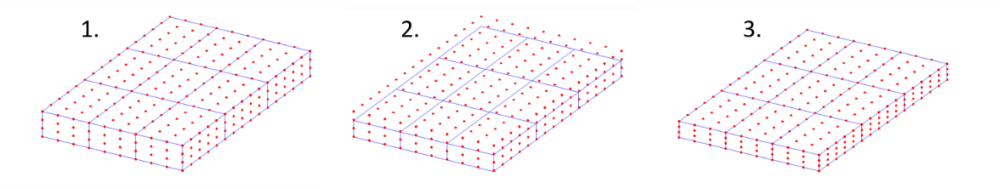

Figure 2: Node mapping process from an initial geometry to a geometry deformation

Optimization framework

The *lightworks* optimization framework [12], which particularly focuses on composite wing structures, is employed to perform the optimization studies in this work. It inherits a variety of gradient-based optimization algorithms, allowing for flexible selection depending on the specific problem at hand.

For structural analysis, a FE model, using smeared panel descriptions is used. This is done by using the *B2000++* FE solver [14] to provide stress distributions and deformations for criteria analyses. This model also provides a basis for deriving a structural model that describes the mechanical properties of the overall structure.

The FE model is divided into optimization regions, each enclosed by ribs and spars. Each region is defined by one panel, which characterizes its stiffness properties. Each panel comprises a composite material description. A continuous stiffness formulation based on lamination parameters is used, which has proven suitable for gradient based optimization [15].

The gradient calculations within *lightworks* follow a modular approach, with separate partial gradients calculated for different code sections. This structure facilitates the use of highly accurate methods like algorithmic differentiation while allowing for approximations using finite differences where such precise methods are not applicable.

Optimization tasks using *lightworks* are typically designed for stability due to buckling and strength. To address these failure types, various criteria are implemented, defining the feasibility. The objective function is the system's mass which should be minimized.

Gradient calculation

Gradients steer the gradient-based optimization algorithm in the direction of the optimum, guiding the search for an optimal solution. For this process, the algorithm requires both gradients of the constraint and objective functions with respect to the design variables. In a monodisciplinary structural optimization context, structural constraint gradients are calculated with respect to structural parameters primarily influencing the system's stiffness.

However, in an MDO, where a variable affects multiple disciplines, these become interdisciplinary parameters. For instance, the wing geometry significantly influences aerodynamic performance but also impacts the structure of the wing. Consequently, such parameters are considered interdisciplinary because they have implications across different disciplines.

Gradients with respect to these parameters are called interdisciplinary gradients. To include these interdisciplinary gradients into *lightworks* the gradient determination process is extended as described below.

The straightforward approach is to calculate these gradients directly using finite differences. However, this method can exhibit numerical errors and can be computationally expensive for a high number of design variables.

lightworks features a modular hierarchical structure that enables the application of various gradient determination methods at different hierarchy levels. Moreover, it supports calculating numerically exact gradients using algorithmic differentiation wherever possible, while still being able to use finite differences when AD is not applicable.

With the addition of interdisciplinary geometric parameters, it becomes necessary to distinguish between gradients with respect to structural and geometrical parameters. Structural parameters affect the structural properties of the system, whereas geometric parameters influence the shape represented by mesh nodes. The gradients of the constraint and objective functions are calculated with respect to these different types of parameters.

Equation 1 and 2 illustrate the calculation of the gradients of the objective f and constraint g functions in relation to both structural x_s and geometric x_g parameters. In this work, the gradients of mesh nodes with respect to geometrical parameters are declared as geometry gradients.

$$\frac{dg(x_s,x_g)}{d\vec{x}} = \begin{pmatrix} \frac{\partial g(x_s,x_g)}{\partial x_s} \\ \frac{\partial g(x_s,x_g)}{\partial x_g} \end{pmatrix} = \begin{pmatrix} \frac{\partial g(x_s,x_g)}{\partial x_s} + \frac{\partial g(x_s,x_g)}{\partial \vec{\sigma}} \frac{\partial \vec{\sigma}(x_s,x_g)}{\partial x_s} \\ \frac{\partial g(x_s,x_g)}{\partial \vec{n}} \frac{d\vec{n}(x_g)}{dx_g} + \frac{\partial g(x_s,x_g)}{\partial \vec{\sigma}} \frac{\partial \vec{\sigma}(x_s,x_g)}{\partial x_g} \end{pmatrix} \quad (1)$$

$$\frac{df(x_s,x_g)}{d\vec{x}} = \begin{pmatrix} \frac{\partial f(x_s,x_g)}{\partial x_s} \\ \frac{\partial f(x_s,x_g)}{\partial x_g} \end{pmatrix} = \begin{pmatrix} \frac{\partial f(x_s,x_g)}{\partial x_s} \\ \frac{\partial f(x_s,x_g)}{\partial \vec{n}} \frac{d\vec{n}(x_g)}{dx_g} \end{pmatrix} \quad (2)$$

where:
$\vec{\sigma}$: internal panel stresses, calculated by the FE solver
$\vec{n}$: node coordinates for each node in x-, y- and z-direction

Each partial gradient can be calculated using different gradient determination methods. The marked entries can be determined numerically exact using an algorithmic differentiation approach. Specifically:

- Blue-marked entries are calculated using the algorithmic differentiation method of the *autograd* package [16].
- Orange-marked entries are computed using the differentiated *OpenCASCADE Technology (AD-OCCT)* package [9].

The AD gradients from the *autograd* package can be calculated using either the forward or reverse method, depending on the number of in- and outputs. In contrast, the *AD-OCCT* package supports only the forward method at this stage. However, since the number of geometry parameters is significantly smaller than the number of nodes, the forward method is inherently more efficient in this case. Consequently, the performance benefit is not expected to come directly from using AD gradients, as the number of evaluations remains the same as using the FD method. Instead, it is expected to come from the subsequent reduction in the number of iterations required due to the high accuracy of the AD gradients.

The unmarked entries in Equations 1 and 2 can only be estimated using finite differences, since the stresses are calculated by the external FE solver *B2000++* [14]. This solver doesn't provide the necessary gradients directly. Therefore, the gradients are calculated by external perturbation. This method is less precise but can still provide useful approximations when exact differentiation methods are not available.

3. Problem formulation

To verify the proposed methodology, a specific use case is selected, used in prior literature for analysing composite optimization issues [12, 17–20]. This case involves a simplified rectangular structure, as shown in Figure 3. This use case represents a simplified wing box. In contrast to the mentioned publications, all panels, including the ribs and spars, are optimized. The entire model is taken into consideration to ensure that the geometry parameters accurately influence the objective function as this might not be the case if not all panels in the model are accounted for.

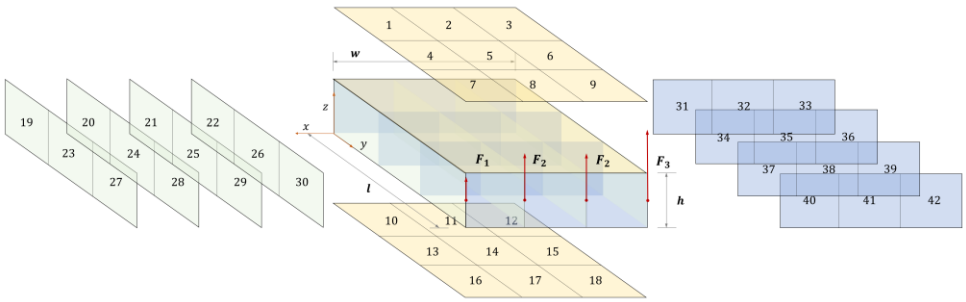

Figure 3: Wing box example use case [12]

The structure is clamped at the root, located at the origin of the coordinate system and subjected to asymmetric loads applied at the tip. Both the upper and lower surfaces are divided into nine optimization regions, bounded by four evenly spaced rib- and spar panels. These panels are composed to a shear layup configuration [(±45°)22]. The panels on both the upper and lower shells of the box are equipped with an axial layup configuration [4(0°)/4(+/-45°)/2(90°)]. The discrete stacking sequences are stored using a continuous lamination parameter formulation. The wing box has a length of 3543 mm, a width of 2240 mm, and a height of 381 mm. The box is subjected to three different forces: F1=90009.77 N, F2=187888.44 N and F3=380176.16 N. The T300/5208 pre-preg material is used for each individual layer [19]. The material properties are summarized in Table 1.

Table 1: Properties of the T300/5208 pre-preg used for optimization studies [19]

Property	Value
E_{xx}	$181GPa$
$E_{yy} = E_{zz}$	$10.3GPa$
$\nu_{xy} = \nu_{xz}$	0.27
ν_{yz}	0.42
$G_{xy} = G_{xz}$	$7.17GPa$
G_{yz}	$3.78GPa$
ρ	$1760\,\frac{kg}{m^3}$
$X_t = X_c$	$1500MPa$
$Y_t = Y_c$	$246MPa$
S	$68MPa$

The objective is to achieve minimal mass while ensuring all stability and strength constraints are met. For stability, a combined compression-shear buckling criterion based on the *Handbook for Aeronautical Engineering (HSB)* [21] ensures that the structure can withstand compressive and shear forces without buckling. The stability constraints are evaluated on panel level, meaning one constraint for each panel. A detailed description of the stability constraint employed is provided in the appendix.

To negate strength failure, a lamination parameter strength criterion is used as described in Khani et al. [22]. This criterion is used to optimize the strength of continuous formulated composite laminates while addressing the limitations of traditional strength criteria, which depend explicitly on ply angles and stacking sequence. Since a lamination parameter definition for the composites is used, no discrete stacking sequence is available. The strength constraints are evaluated on element level resulting in one strength constraint for each element in the FE model.

The optimization algorithm employed is the *Sparse Nonlinear Optimizer (SNOPT)* [23]. The relevant algorithm options used here are summarized in Table 2 in the appendix.

The general optimization problem can be stated as follows, where x_s are structural design variables, x_g geometrical design variables, g_s structural constraints and f the objective function to minimize:

$$\begin{aligned} &\underset{x}{minimize} && f(x_s, x_g) \\ &\text{such that} && x_{s,i}^l \leq x_{s,i} \leq x_{s,i}^u i = 0, \dots, n_s \\ & && x_{g,j}^l \leq x_{g,j} \leq x_{g,j}^u j = 0, \dots, n_g \\ &\text{subject to} && g_{s,k}(x_s, x_g) \leq 0 k = 0, \dots, m \end{aligned}$$

4. Results

This section shows the application of the aforementioned process and their adaptions. The rectangular wing box structure described in Section 3 is optimized without changing the geometry at first. Subsequently, the gradient estimation methods are investigated by comparing AD and FD geometrical gradients. Due to the fact that the wing box geometry is quite simple, analytical gradients can be calculated. These serve to verify the implantation and determine errors of the gradient determination methods. Afterwards, the height of the box is provided as a design parameter to the optimization algorithm. The geometry gradients in this optimization are calculated using AD. The results are compared to the structural-only optimization. The impact of the geometry gradient determination method on the convergence rate of optimization is examined by applying FD method to the combined structural and geometric optimization. The convergence rate is then compared to that achieved using AD geometric gradients.

Structural-only optimization

To structurally optimize the previously described wing box, the thickness of each panel is optimized. One stability constraint is evaluated for each panel, while a strength constraint is assessed for each element. Overall, this results in 42 stability and 558 strength constraints that need to be considered by the optimization algorithm. This optimization yields a mass of 343.36 kg for the complete wing box.

Figure 4 shows the mass breakdown for each component from this optimization compared to the reference literature. The mass is increased by 10.42% in comparison to the reference. This is due to the fact that only the thicknesses were optimized here, while the composite material itself remained

unchanged. Consequently, the components cannot be designed for an optimal layup design, leading to stability and strength improvements solely through increased thickness. Therefore, the upper and lower shells have greater masses. In contrast, the ribs and spars are slightly lighter because they were considered in the optimization.

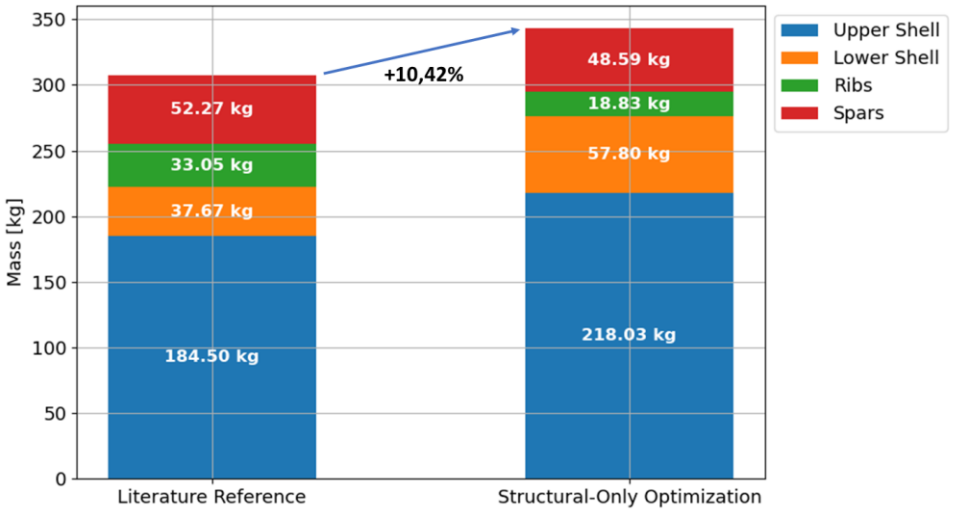

Figure 4: Comparison between the optimized masses of each wing component from the structural-only optimization and the literature reference [12]

The upper panels are critical for buckling, whereas the lower panels are critical for strength. The optimizer converges in 15 iterations, as shown in Figure 5. The resulting optimal solution features a maximum constraint value of $8.41e^{-5}$, which is within the given numerical tolerance.

In the initial step, the optimizer makes a significant reduction in the wing box's mass. This drastic change is coupled with an increase in constraints, which pushes the design towards higher constraints. Subsequently, the mass starts to increase, while the constraints gradually guide the design toward a feasible solution. Finally, the design achieves feasibility within the specified numerical tolerances of 10^{-3}.

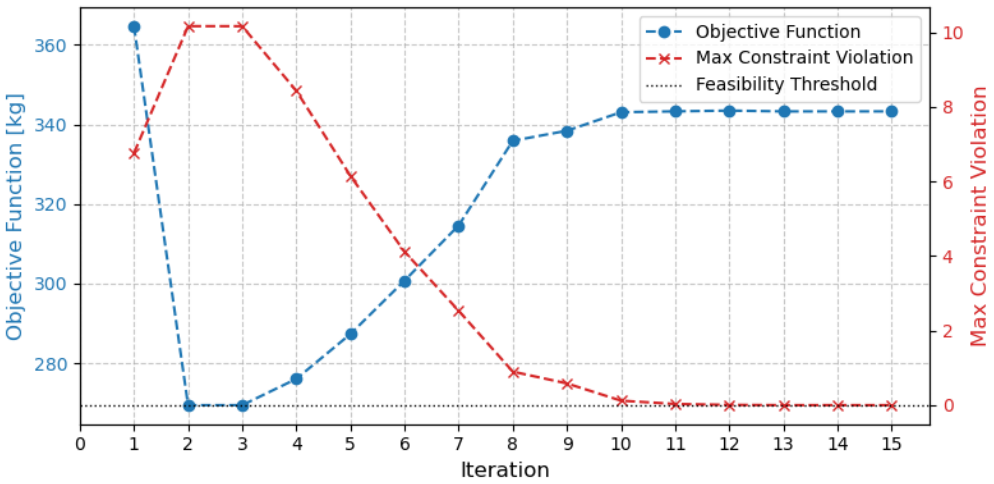

Figure 5: Convergence plot of the structural-only optimization

The optimization algorithm is successfully identifying a structurally feasible solution with minimal mass by adjusting the panel thicknesses. *SNOPT* ensures feasibility by enforcing constraints within the predefined feasibility tolerance. The solution satisfies all structural constraints.

Comparison of geometry gradients using the AD and FD method

On this specific use case, the mismatch error between the AD and FD gradient determination methods is evaluated. Analytical exact gradients serve as a reference.

The analytical gradients can be calculated using the following equations. However, this applies only to this specific use case where the profile height serves as a design variable. The relationship between the maximum node position in the z-direction and the profile height is given by

$$h = n_{z,max} \tag{3}$$

The gradient value depends on the node's position in the z-direction. Substituting this into the equation results in:

$$n_z = \frac{n_z}{n_{z,max}} \cdot h \tag{4}$$

Thus, in this case, the geometry gradient is:

$$\frac{dn_z}{dh} = \frac{n_z}{n_{z,max}} \tag{5}$$

This constrains the gradients to always remain between 0 and 1, depending on the z-positioning of the nodes.

Figure 6 represents the absolute error between the AD and FD method on a logarithmic scale. The grey line represents the machine accuracy. Everything below this line can be considered as numerically exact. The comparison is made for each degree of freedom, with each point in the plot representing one node of the FE model. Darker spots indicate clusters of points.

For the AD gradients in both the x and y directions, all errors are below the line of machine accuracy of $2.22e^{-16}$. However, in the z direction, only a few points exceed this line by a small amount, with the maximum error reaching $5.55e^{-16}$.

In contrast, for the FD methods, larger errors can be observed. In the x direction, some gradients are calculated numerically exact. However, many points exhibit significant differences compared to the analytical gradients. Here, the maximum error is approximately 0.016, with roughly 25.8% of nodes having this level of inaccuracy. For the z direction, all geometry gradients exhibit errors but are generally smaller than those in the x direction.

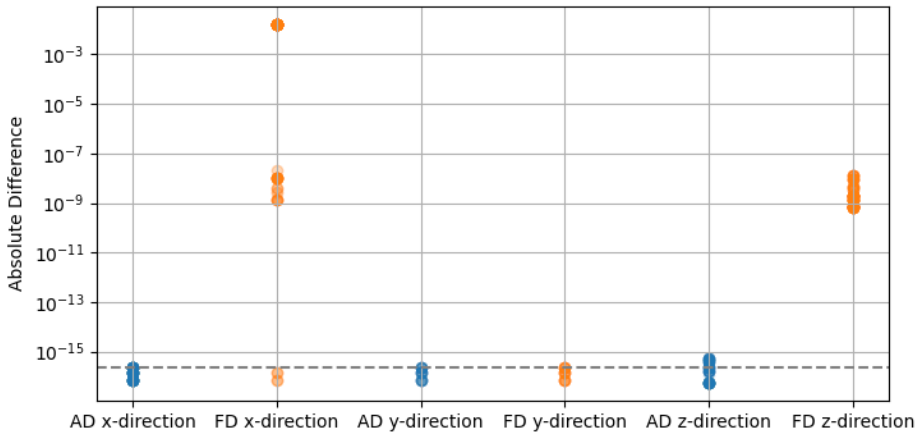

Figure 6: Absolute difference of AD and FD geometry gradients compared to exact analytical gradients

The differences in geometry gradients lead to variations in the overall relative error of all constraint gradients, as illustrated in the plot shown in Figure 7. This comparison was made by evaluating the overall constraint gradients using

AD for the geometry gradients as one dataset and FD methods for the geometry gradients as another dataset.

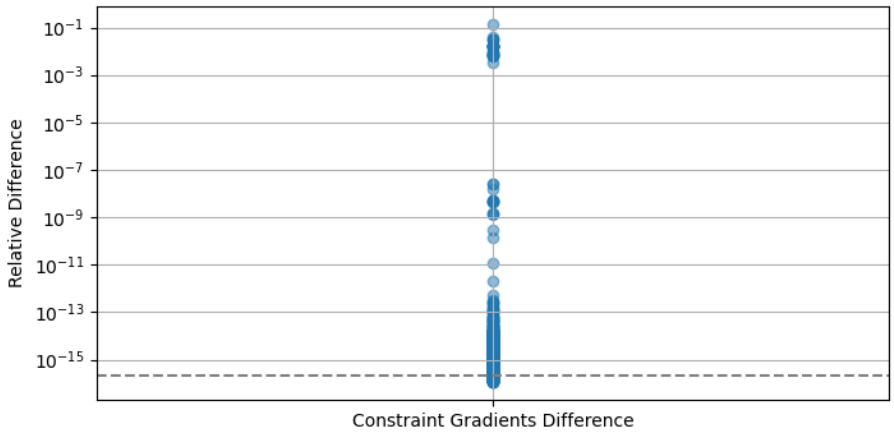

Figure 7: Relative difference of constraint gradients using AD and FD geometry gradients

It is assumed that the first dataset, which uses AD for almost all partial gradients as listed in Equations 1 and 2, returns the most accurate results. However, the solver gradients, marked as black in these equations are computed using FD, since AD methods are not available for those. Therefore, some errors are still expected.

To ensure the relative error is attributed to the geometry gradients only, the exact same solver gradients for both datasets are used. This approach allows to isolate and compare the effects of the geometry gradients on the overall constraint gradients.

The maximum relative error observed is 0.1365, indicating a significant disparity in some cases. However, the vast majority of the 600 constraints show minimal relative errors. Specifically, only 4.5% of all constraints have a relative error greater than $1e^{-3}$. The discrepancy on the objective gradient with respect to the profile height between AD and FD is $6.86e^{-9}$. It is evident that an error arises when using FD geometry gradients.

Combined optimization of structure and geometry using AD geometry gradients

To demonstrate the applicability of interdisciplinary parameters in structural optimization, a combined structural-geometric optimization is conducted. The results from this approach are then compared to those obtained from the structural-only optimization.

In this optimization process, the thicknesses of each panel and the profile height h, as shown in Figure 3, are simultaneously optimized. The result obtained from this optimization is then compared with those from the pure structural optimization, which only involved the panel thicknesses. The objective and geometry gradients where calculated using algorithmic differentiation in the case of the combined optimization since they employ no numerical errors as shown previously.

With the combined optimization, the optimization algorithm successfully reduced the mass of the wing box further by 1.1%, bringing it down to 338.16 kg. The profile height was increased by 26.5% from 0.381 meters for the wing box baseline to 0.482 meters for the optimized design. A comparison between the initial profile height and the optimized profile height is visualized in Figure 8.

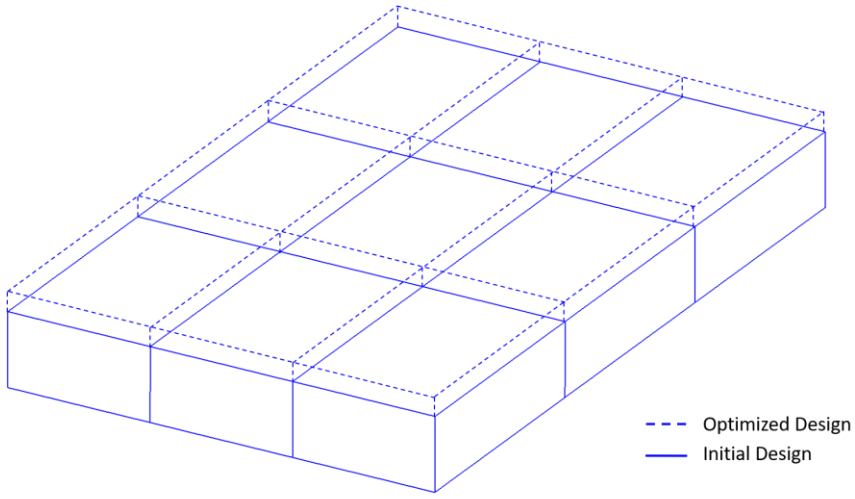

Figure 8: Comparison between the initial wing box design and the profile height optimized design

To illustrate the influence of profile height on structural mass, thickness-only optimizations at various fixed profile heights are conducted and the final optimized mass against these different heights is shown. This allows to visually identify the influence of the profile height on the structural mass in the combined optimization. The optimal height in Figure 9 of approximately 0.48 meters aligns with the findings of this optimization study.

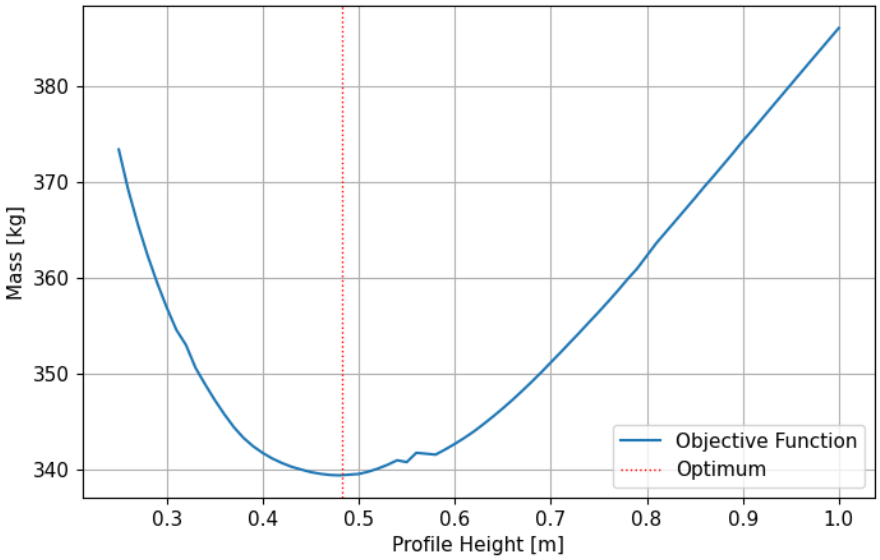

Figure 9: Influence of the profile height on the structurally optimized mass of the wing box

Two primary effects are evident when examining this plot. First, for lower profile heights, there is a significant increase in structural mass. This can be attributed to the moment of inertia's relationship with maximum displacement and therefore the internal loads applied to the panels. The maximum displacement δ is inversely proportional to the moment of inertia I (Equation 6). As the profile height increases, the reduction in mass follows a cubic relationship due to the moment of inertia's dependence on the cube of the height as shown in Equation 7. This means, as the profile height gets significantly larger, the rate of decrease in structural mass slows down and eventually levels off.

$$\delta \propto \frac{1}{I} \tag{6}$$

$$I = \frac{bh^3}{12} \tag{7}$$

This effect can be demonstrated by plotting the maximum displacements of the wing box baseline with different profile heights as shown in Figure 10.

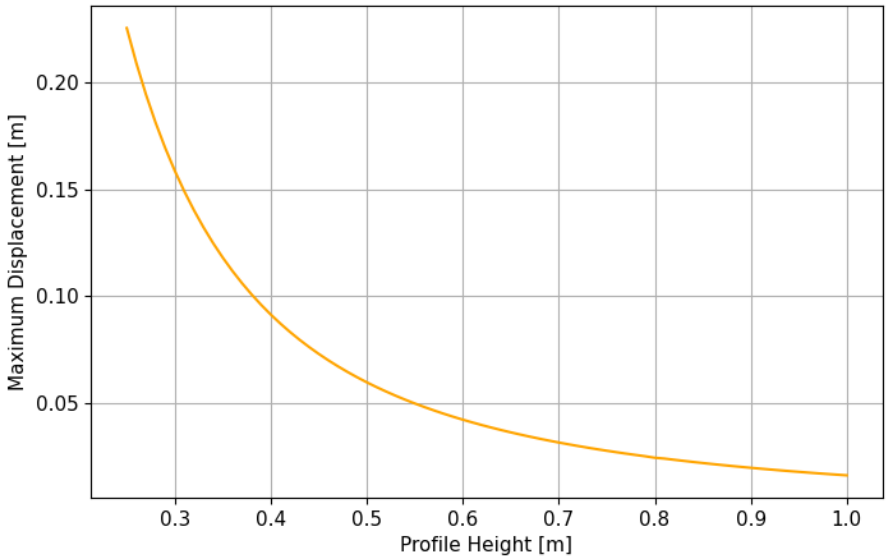

Figure 10: Influence of the profile height on the maximum displacement of the wing box

Conversely, another effect becomes dominant as the profile height increases, where the structural mass increases linearly in this case. At lower profile heights, this linear increase is overshadowed by the influence of the moment of inertia. However, as the profile height continue to rise, the linear increase in mass becomes more pronounced and begins to dominate.

Combining these two effects results in the progression shown in Figure 9. The optimal profile height minimizes both the high internal loads at low heights and the unnecessary mass added by excessively large profiles.

Figure 11 illustrates the mass breakdown of each wing component for the structural-only and combined optimization. It shows a shift in the distribution of mass within the structure. It is evident that both the lower and upper shell masses have been reduced. However, this mass saving is reduced by an increase in the masses of the ribs and spars, primarily due to the higher profile height. Due to the different sensitivities of the covers and inner structure, the overall mass of the wing is still reduced by 1.1%.

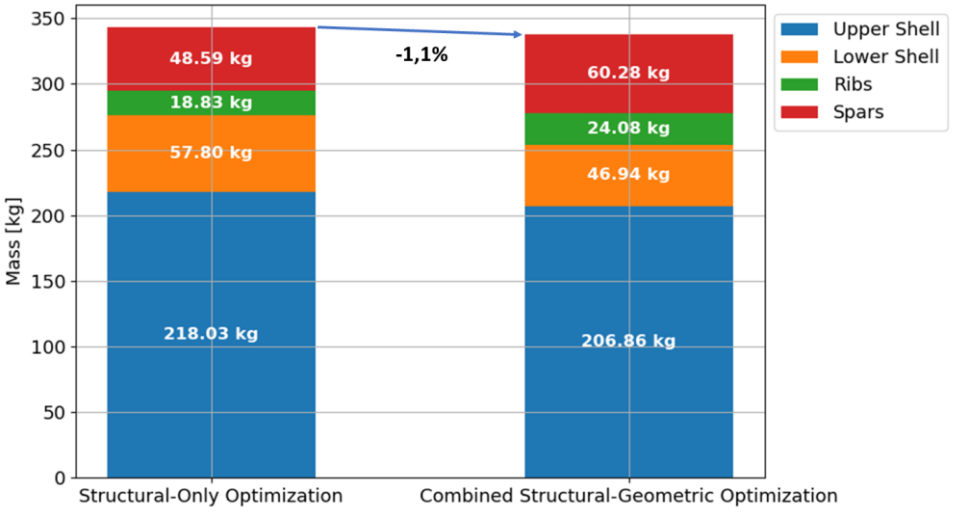

Figure 11: Mass breakdown of the structural-only and combined structural-geometric optimized design

The convergence plot of this optimization is shown in Figure 12, illustrating that it converges within 58 iterations. Notably, there is a spike observed in the maximum constraint value during the process. This can be explained by the significant reduction in thickness of the central lower panel, which has caused the maximum constraint to shift to that particular region.

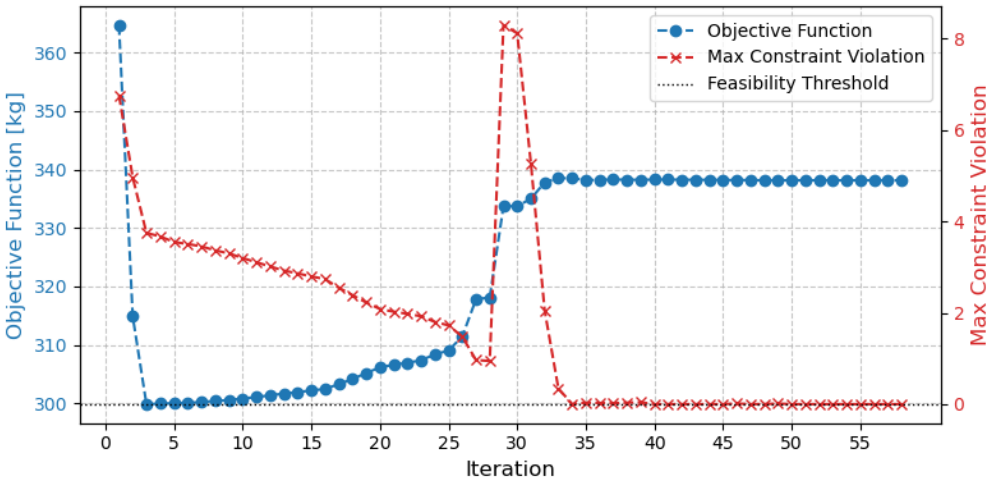

Figure 12: Convergence plot of the coupled structural-geometric optimization using AD geometry gradients

Influence of FD geometry gradients on the convergence rate

The influence on the convergence rate when employing AD gradients as opposed to FD gradients is investigated. Here, the same combined structural-geometric optimization process is conducted, using FD geometry gradients instead of AD.

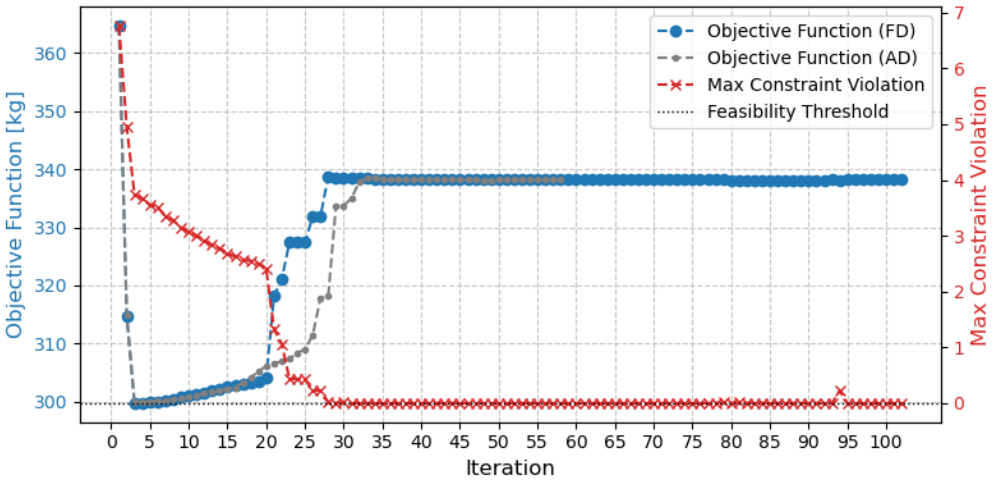

Figure 13: Convergence plot of the coupled structural-geometric optimization using FD geometry gradients

Both optimizations result in nearly the same mass. However, the convergence rate, shown in Figure 13, was found to be different for the two optimization runs. The run using finite differences needs more iterations to reach the termination criterion compared to the run with exact gradients. This difference can be attributed to the inexact nature of finite differences.

In both cases, the same *SNOPT* options were used, so any differences in convergence behavior can be attributed to the gradient calculation method of the geometry gradients.

While the choice of gradient calculation method does not significantly impact the final mass, it does have an effect on the convergence rate and the behavior of the optimization algorithm.

5. Conclusion

Multidisciplinary optimizations have paved the way for more efficient aircraft designs. To achieve these optimizations, interdisciplinary gradients that reflect interactions between different disciplines are crucial. One key area is geometry changes and their impact on structural integrity. Usually those geometric

parameters are associated to the aerodynamic discipline. A CAD-based shape optimization approach can ensure consistency across multiple disciplines by utilizing centralized CAD data.

The profile height showed a potential to reduce the box mass, despite neglecting the aerodynamic effects. Gradients of structural constraint and objective functions with respect to geometrical parameters can be determined. Through these gradients, it is possible to couple the aerodynamic and structural discipline, enabling MDO.

This approach was successfully integrated into the *lightworks* optimization framework, enabling mass optimization using any geometric design variable while maintaining structural integrity.

The errors of numerical exact AD and approximated FD geometric gradients are investigated. Compared to analytical gradients, the FD gradients exhibit significant inaccuracies in certain cases. In contrast, AD gradients are numerically exact, with errors being below machine precision.

The discrepancies in the gradient determination methods become apparent when comparing their convergence rates. Optimization using AD geometry gradients reaches the termination criteria faster than FD gradients. However, this can be neglected by loosening the termination tolerance. In this simple use case, where geometry gradients are linearly related to design variables, the numerical errors from FD are not significant for the optimization algorithm. Applying this methodology to more complex scenarios would make the benefits of using AD gradients more evident.

In the scope of this research, the structural discipline was primally focused. However, it is important to note that for a truly comprehensive MDO approach, consideration must be given to other disciplines as well. In the context of geometric wing optimization, it is essential to account for aerodynamic performance, not just structural aspects. Despite this, the gradients related to structural constraints and objective functions can be derived with respect to geometric parameters, thereby narrowing the gap in coupling structure and aerodynamics.

Using a CAD-based approach allows for the positional optimization of internal components as well. Optimizing the inner structure through positioning ribs and spars may lead to favorable deflections in the wing, thereby alleviating loads and minimizing structural mass requirements. However, this process requires establishing constraints to prevent overlap and other constraints.

In summary, while finite differences might be sufficient for simpler geometries, algorithmic gradients have a significant advantage in more complex scenarios, which shows the demand of algorithmic differentiation.

Appendix

Stability buckling constraint

The critical buckling load for compression $n_{x,cr}$ found in HSB 45111-08, Issue C and shear $n_{xy,cr}$, HSB 45112-02, Issue C, are calculated as shown in Equations 8 and 9.

$$n_{x,cr} = k_x(\overline{\alpha}, \beta) \cdot \left(\frac{\pi}{b}\right)^2 \cdot \sqrt{\widetilde{D}_{11} \cdot \widetilde{D}_{22}} \tag{8}$$

$$n_{xy,cr} = k_{xy}(\overline{\alpha}, \beta) \cdot \left(\frac{\pi}{b}\right)^2 \cdot \sqrt[4]{D_{11} \cdot D_{22}^3} \tag{9}$$

where k_x and k_{xy} are the buckling coefficients for compression and shear respectively. These coefficients are calculated using the effective aspect ratio of the panel $\overline{\alpha}$and Seydel's orthotropy parameter β and are dependent on the support conditions of the panel. Here, b stands for the buckling width of the panel and D_{ij} for the bending stiffness. For the compression buckling, $\widetilde{D}_{ij}$ refers to a corrected bending stiffness in case when the coupling stiffness B is not zero. However, for symmetric orthotropic plates is $\widetilde{D}_{ij} = D_{ij}$.

Both compression and shear buckling can be combined into one expression using Equation 10.

$$R = \left(\frac{n_{xy,cr}}{n_{xy}}\right)^2 + \frac{n_{x,cr}}{n_x} \leq 1 \tag{10}$$

Using this combined expression, a single constraint value can be calculated using Equation 11, where a value smaller than zero is considered as feasible.

$$g = \frac{1}{R} - 1 \tag{11}$$

SNOPT options

Table 2: Used SNOPT options

Option	Value
Derivative level	3
Linesearch tolerance	0.97
Major feasibility tolerance	$1e^{-3}$
Major optimality tolerance	$1e^{-3}$
Minor feasibility tolerance	$1e^{-3}$
Scale option	0
Nonderivative linesearch	$True$

6. References

[1] D. P. Raymer, *Enhancing aircraft conceptual design using multidisciplinary optimization / by Daniel P. Raymer*. [Stockholm, Sweden]: [Royal Institute of Technology], 2002.

[2] J. R. R. A. Martins und A. B. Lambe, "Multidisciplinary Design Optimization: A Survey of Architectures," *AIAA Journal*, Jg. 51, Nr. 9, S. 2049–2075, 2013, doi: 10.2514/1.J051895.

[3] J. A. Samareh, "Survey of Shape Parameterization Techniques for High-Fidelity Multidisciplinary Shape Optimization," *AIAA Journal*, Jg. 39, Nr. 5, S. 877–884, 2001, doi: 10.2514/2.1391.

[4] G. Kenway, G. Kennedy und J. R. R. A. Martins, "A CAD-Free Approach to High-Fidelity Aerostructural Optimization," in *13th AIAA/ISSMO Multidisciplinary Analysis Optimization Conference*, Fort Worth, Texas, 2010, doi: 10.2514/6.2010-9231.

[5] B. J. Brelje und J. R. Martins, "Aerostructural Wing Optimization for a Hydrogen Fuel Cell Aircraft," in *AIAA Scitech 2021 Forum*, VIRTUAL EVENT, 2021, doi: 10.2514/6.2021-1132.

[6] X. He, J. Li, C. A. Mader, A. Yildirim und J. R. Martins, "Robust aerodynamic shape optimization—From a circle to an airfoil," *Aerospace Science and Technology*, Jg. 87, S. 48–61, 2019, doi: 10.1016/j.ast.2019.01.051.

[7] G. K. W. Kenway und J. R. R. A. Martins, "Multipoint Aerodynamic Shape Optimization Investigations of the Common Research Model

Wing," *AIAA Journal*, Jg. 54, Nr. 1, S. 113–128, 2016, doi: 10.2514/1.J054154.

[8] H. Hajdik, A. Yildirim und J. R. Martins, "Aerodynamic Shape Optimization with CAD-Based Geometric Parameterization," in *AIAA SCITECH 2023 Forum*, National Harbor, MD & Online, 01232023, doi: 10.2514/6.2023-0726.

[9] M. Banović, O. Mykhaskiv, S. Auriemma, A. Walther, H. Legrand und J.-D. Müller, "Algorithmic differentiation of the Open CASCADE Technology CAD kernel and its coupling with an adjoint CFD solver," *Optimization Methods and Software*, Jg. 33, 4-6, S. 813–828, 2018, doi: 10.1080/10556788.2018.1431235.

[10] OpenCASCADE. "OpenCASCADE Technology." Accessed: 27. Januar 2025. [Online.] Available at: https://www.opencascade.com/

[11] J. Kleinert, A. Reiswich, M. Banovic und M. Siggel, "A Generic Parametric Modeling Engine Targeted Towards Multidisciplinary Design: Goals and Concepts," *CADandA*, S. 424–443, 2023, doi: 10.14733/cadaps.2024.424-443.

[12] S. Dähne, E. Werthen, D. Zerbst, L. Tönjes, H. Traub und C. Hühne, "Lightworks, a scientific research framework for the design of stiffened composite-panel structures using gradient-based optimization," *Struct Multidisc Optim*, Jg. 67, Nr. 5, 2024, doi: 10.1007/s00158-024-03783-1.

[13] C. Geuzaine und J.-F. Remacle, "Gmsh: A 3-D finite element mesh generator with built-in pre- and post-processing facilities," *Numerical Meth Engineering*, Jg. 79, Nr. 11, S. 1309–1331, 2009, doi: 10.1002/nme.2579.

[14] SMR SA, *B2000++: Finite Element Analysis Environment.* [Online]. Available at: https://www.smr.ch/products/b2000/

[15] K. R. Bramsiepe, V. Handojo, Y. M. Meddaikar, M. Schulze und T. Klimmek, "Loads and Structural Optimization Process for Composite Long Range Transport Aircraft Configuration," in *2018 Multidisciplinary Analysis and Optimization Conference*, Atlanta, Georgia, 06252018, doi: 10.2514/6.2018-3572.

[16] D. Maclaurin, D. Duvenaud, M. Johnson und J. Townsend, *Autograd.* [Online]. Available at: https://github.com/HIPS/autograd

[17] B. Liu, R. T. Haftka und M. A. Akgün, "Two-level composite wing structural optimization using response surfaces," *Struct Multidisc Optim*, Jg. 20, Nr. 2, S. 87–96, 2000, doi: 10.1007/s001580050140.

[18] D. Liu, V. V. Toroporov, O. M. Querin und D. C. Barton, "Bilevel Optimization of Blended Composite Wing Panels," *Journal of Aircraft*, Jg. 48, Nr. 1, S. 107–118, 2011, doi: 10.2514/1.C000261.

[19] M. P. Scardaoni und M. Montemurro, "A general global-local modelling framework for the deterministic optimisation of composite structures," *Struct Multidisc Optim*, Jg. 62, Nr. 4, S. 1927–1949, 2020, doi: 10.1007/s00158-020-02586-4.

[20] D. Zerbst, L. Tönjes, S. Dähne, E. Werthen, E. Kappel und C. Hühne, "Equivalent plate formulation of Double–Double laminates for the gradient-based design optimization of composite structures," *Composite Structures*, Jg. 354, S. 118786, 2025, doi: 10.1016/j.compstruct.2024.118786.

[21] Working group Structural Analysis (IASB), *Aeronautical Engineering Handbook (LTH): Handbook for structural analysis (HSB)*.

[22] A. Khani, S. T. IJsselmuiden, M. M. Abdalla und Z. Gürdal, "Design of variable stiffness panels for maximum strength using lamination parameters," *Composites Part B: Engineering*, Jg. 42, Nr. 3, S. 546–552, 2011, doi: 10.1016/j.compositesb.2010.11.005.

[23] P. E. Gill, W. Murray und M. A. Saunders, "SNOPT: An SQP Algorithm for Large-Scale Constrained Optimization," *SIAM Rev.*, Jg. 47, Nr. 1, S. 99–131, 2005, doi: 10.1137/S0036144504446096.